(Received 21 October 2024, Accepted 28 November 2024, Scheduled 11 December 2024)

Design and Analysis of Linear Primary Permanent Magnet Vernier Machines with Different Winding Configurations

Zhijian Ling, Qi Zhang, and Meimei Xu*

School of Electrical and Information Engineering, Jiangsu University, Zhenjiang 212013, China

ABSTRACT: This paper investigates the effects of winding configurations on force density and fault tolerance in linear primary permanent magnet vernier (LPPMV) machines. Firstly, the LPPMV machines with integral slot distributed windings (ISDWs) and fractional slot concentrated windings (FSCWs) are discussed. Due to the high modulation ratio of ISDW machine, it has the potential to achieve higher thrust force capabilities. Then, the operation principle of the LPPMV machines is analyzed from the perspective of air-gap magnetic modulation. Furthermore, it should be noted that the winding configurations of ISDW machine has larger spans, resulting in insufficient fault-tolerance. To solve this limitation, a new modular ISDW LPPMV machine was proposed and optimized. In the modular ISDW LPPMV machine, a 3×3-phase winding configuration is employed. It is demonstrated that modular ISDW LPPMV machines exhibit superior characteristics in both thrust density and fault tolerance. Finally, the experiments are carried out in a linear test bench, verifying the theoretical analysis.

1. INTRODUCTION

Linear machine achieves the direct conversion of electromagnetic energy into linear mechanical energy without the need for intermediate transmission or conversion devices. They have a wide range of applications in industrial manufacturing, especially in rail transportation, which requires high-performance linear motion [1–3]. Although linear induction machines have been widely used due to their mature technology and low cost, they still face the problem of low thrust and efficiency [4, 5]. In recent years, due to the breakthroughs in the performance of PM materials and innovations in topology structures, LPPMV machines which provide higher thrust force have received increasing attention [6, 7].

Based on the principle of magnetic field modulation, the LPPMV machine utilizes the "magnetic gear effect" of unequal pole numbers between the armature winding poles and PM array poles to achieve a higher thrust force [8, 9]. It has excellent application prospects in rail traction systems. Notably, both the windings and PMs of the LPPMV machine are mounted on the mover [10, 11]. Consequently, the utilization of costly PM materials is minimized, thereby leading to reduced expenses for long-stroke operations, and the design complexity of the machine structure is significantly streamlined.

As the demand for practical applications rises, it is crucial to further enhance the thrust density of LPPMV machines. In [12], by increasing the cooling equipment or using improved cooling mediums and heat dissipation structures, the electrical load of LPPMV machines can be increased from one to three times of the original, significantly enhancing the thrust density. However, the lifespan of the machine could be potentially reduced due to the exacerbation of the primary heating caused by escalating the electrical load. This increased thermal stress could potentially lead to short-circuit faults and even cause direct damage to the machine. Besides, the PMs can be optimized by utilizing Halbach array magnets, V-shaped magnets, spoke-type magnets, or similar concentrated magnetic types. It is possible to effectively enhance working magnetic flux density of the machine and improve thrust density [13]. As discussed in [14, 15], a surface-mounted PM linear machine with a Halbach array magnet further increases thrust density of linear machine. However, the Halbach design requires strong forces to press blocks with different magnetic field orientations together, thus potentially increasing susceptibility to demagnetization due to strong stresses and fluctuating magnetic field directions. In [16], a double-sided stator PM linear machine is proposed, which not only effectively reduces the machine weight and enhances the thrust density but also reduces the copper losses and volume of the machine, thereby improving efficiency. However, the implementation of a dual-sided structure is poised to increase the complexity of both manufacturing processes and maintenance procedures [17].

To further enhance the high thrust force advantages of LPPMV machines, high modulation ratio designs can be employed [18, 19]. In [20], the performance difference of PM rotary machines with ISDWs and FSCWs has been discussed. Distributed windings with a lower effective pole pair count increase the modulation ratio, improving the utilization of the magnetic field [21]. However, there is not much literature on this in linear machines. In order to further verify the correctness of the theory in linear machines, some analyses should be carried out, which is meaningful. In magnetically modulated machines, the number of slots per pole per phase correlates positively with the modulation ratio [22, 23]. A

* Corresponding author: Meimei Xu (xmm0508@ujs.edu.cn).

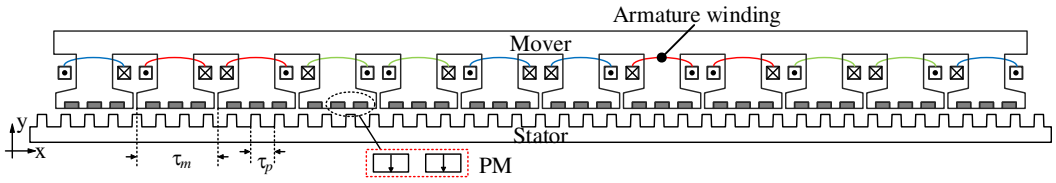

FIGURE 1. Configuration of FSCW machine.

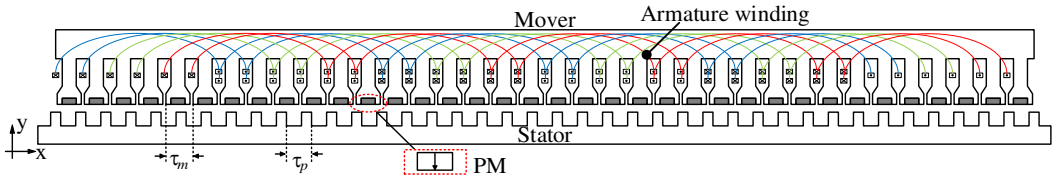

FIGURE 2. Configuration of ISDW machine.

higher modulation ratio necessitates a larger span for distributed windings, resulting in strong inter-phase coupling due to overlapping windings and physical contact between coils in different phases. Consequently, a fault in one phase may propagate to other phases [24]. For conventional three-phase machine drives, a single fault in any part of the drive will result in complete failure. Therefore, enhancing the fault tolerance performance of linear motors with distributed windings is necessary [25, 26].

In this article, an LPPMV machine with distributed winding is presented. Due to the high modulation ratio design, the thrust force is significantly higher than that of traditional LPPMV machines with concentrated winding. Additionally, to achieve multiple sets of spatially independent windings, the edge characteristics of linear machines are utilized to alter the winding configuration. This approach ensures a high modulation ratio while providing certain fault-tolerant capabilities for distributed winding LPPMV machines. In Section 2, the topology of a traditional FSCW machine and proposed ISDW machine is introduced. The topologies and operation principles of the two machines are explained based on magneto-motive forces (MMF)-permeance models, and then their performances are briefly compared. In Section 3, a new fault-tolerant winding connection is proposed. In Section 4, a comprehensive analysis of the fault tolerance performance of ISDW machines is conducted. The experimental data will be presented in Section 5. Finally, conclusions are drawn in Section 6.

2. TOPOLOGY AND OPERATION PRINCIPLE

The topology of the conventional LPPMV machine is show in Fig. 1, consisting of a mover and a stator. The mover consists of 12 large armature teeth and 36 PMs. There are several split teeth interspersed between them. Each armature tooth is uniformly equipped with three PMs magnetized vertically. The stator structure is a relatively simple structure, with only 41 modulation teeth. The concentrated winding design results in a smaller modulation ratio of only 8.2, hindering the full utilization of the magnetic field and making it challenging to improve thrust force. The ISDW LPPMV machine having 36 armature teeth on the mover is shown in Fig. 2. The total number of the PMs is also 36, with each armature tooth housing a PM magnetized vertically, which ensures that the electromagnetic load is consistent with the traditional LPPMV machine. There are 39 modulation teeth on the stator. The number of armature magnetic field pole pairs is 3, making it easier to achieve a high modulation ratio, which can reach 13. Besides, the winding factor of ISDW machine is 0.966, which is higher than 0.933 for FSCW machine. The enhancement of both high modulation ratio and winding factor leads to higher back electromotive force (EMF), enabling the machine to achieve greater thrust force. Detailed parameter comparisons of the two machines are presented in Table 1.

TABLE 1. Parameters of two machines.

Parameters	FSCW	ISDW
Mover pole pitch τ_m (mm)	52.5	17.5
Mover slot opening b_{s0} (mm)	2.5	2
Stator pole pitch τ_s (mm)	15.4	16.2
Axial lamination length L_1 (mm)	120	120
Number of stator teeth P_s	41	39
Number of the permanent magnets P_{PM}	36	36
Number of armature winding P_w	5	3
Modulation ration G_r	8.2	13
Rated current I (A)	5	5
Rated speed v (m/s)	1.5	1.5
PM width b (mm)	9	4
PM thickness a (mm)	4	4
Self-inductance (mH)	120.586	100.646
Mutual-inductance (mH)	10.01	31.443
Self-inductance/Mutual-inductance (%)	8.3	31.2

2.1. Permanent Magnet Magneto-Motive Force

In order to analyze the internal mechanism that improves thrust force and elucidates the modulation mechanism, the air-gap flux density in LPPMV machines is analyzed using the equiv-

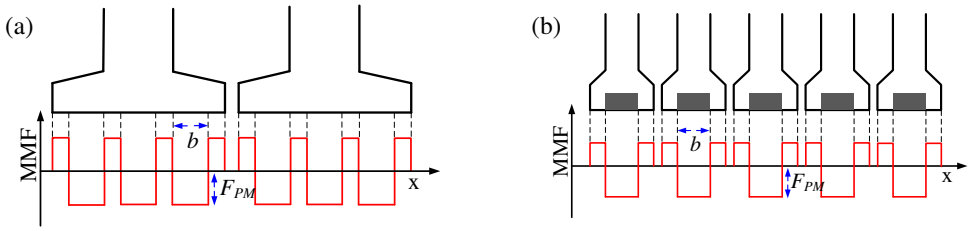

FIGURE 3. PM MMF of two machines. (a) FSCW. (b) ISDW.

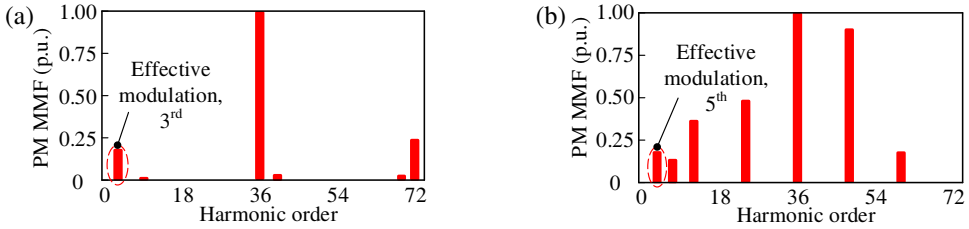

FIGURE 4. Spatial harmonics of PM MMF. (a) FSCW. (b) ISDW.

alent magnetic circuit method. Therefore, in this paper, PM is considered equivalently as a constant magnetic field source. The secondary tooth structure can be regarded as constant permeance. Thus, an equivalent magnetic circuit model for the machine can be derived. To derive the air-gap density of LPPMV machines, it is necessary to establish MMF and permeance models. Before proceeding, the following assumptions are made: 1) the magnetic permeability of the mover and stator is infinite, that is to say neglecting magnetic saturation of the machine core; 2) the permeability in all directions of the PM is equal to air; 3) neglecting the magnetic leakage of the machine; 4) the magnetic field of the machine only varies in the vertical direction; 5) PM MMF is assumed to be square wave. The purpose of this established analytical model is to prominently show the harmonic orders of the air-gap field and corresponding velocities, as well as to reveal the modulation effect of the salient stator. However, it cannot precisely predict the amplitude of the air-gap field or consequently the electromagnetic thrust force. Accurate calculations of the air-gap flux density and electromagnetic thrust force will be carried out using Finite Element Method in later stage.

Figure 3 shows the PM MMF waveform of the two machines. The results show that the magnetic potential waveform of the FSCW machine consists of 6 basic units, each of which can be regarded as a period. However, the MMF waveform of the ISDW machine contains 36 base units, and each base unit can be considered as a period. Different permanent magnet array distributions result in different permanent magnet dynamic waveforms.

2.1.1. PM MMF of FSCW Machine

As shown in Fig. 3(a), the Fourier series expansion of the PM MMF for FSCW can be expressed as

$$F(x) = F_0 + \sum_{i=1}^{\infty} F_i \cos\left(2\pi i \frac{N_s}{L_0} x\right) \tag{1}$$

where

$$\begin{cases} F_0 = N_s F_{PM} \frac{b}{L_0} \\ F_i = \frac{2F_{PM}}{i\pi} \sin\left(\pi i N_s \frac{b}{L_0}\right) \sum_{k=1}^{\infty} (-1)^{k+1} \cdot \\ \cos\left(\pi i N_s (2k-1) \frac{b}{L_0}\right) \end{cases} \tag{2}$$

where N_s is the number of elementary units of FSCW machine, L_0 the effective length of the stator, b the width of PMs, and F_{PM} the amplitude of MMF.

One PM elementary contains three adjacent PMs and four split teeth, on one armature tooth. Each PM elementary unit can be regarded as one period, and the FSCW machine consists of N_s periods.

2.1.2. PM MMF of ISDW Machine

Due to the different machine structures as well as PM distribution between the FSCW and ISDW machines, the PM MMF waveforms of the two machines are different. As shown in Fig. 3(b), the Fourier series expansion of the PM MMF for ISDW machine can be expressed as

$$F(x) = F_0 + \sum_{n=1}^{\infty} F_n \cos\left(2\pi n \frac{P_m}{L_0} x\right) \tag{3}$$

where

$$\begin{cases} F_0 = 0 \\ F_n = -\frac{4F_{PM}}{n\pi} \sin\left(\frac{n\pi}{2}\right) \end{cases} \tag{4}$$

where P_m is the numbers of elementary units of ISDW machine. Due to the effective length of the stator of two machines with the same size, L_0 is applied to both machines.

Figure 4 shows the spatial harmonics of the PM MMF in the air gap of two machines. Fig. 4(a) indicates that the PM MMF of the FSCW machine mainly consists of iN_s harmonic

orders, and i takes positive integers. Besides, the 36th and 48th harmonics dominate the spatial harmonics of FSCW machine. Fig. 4(b) reveals the PM MMF of the ISDW machine composed of nP_m and $3n$ harmonics, where n takes positive odd integers. It can also be clearly seen that the 36th harmonic is dominant.

2.2. Permeance and Air-Gap Flux Density

Because the FSCW and ISDW linear machines have the same stator structure, their permeance models are identical as shown in Fig. 5 and can be expressed as

$$\lambda(x,t) = \lambda_0 + \sum_{j=1}^{\infty} \lambda_j \cos\left[jP_s \frac{2\pi}{L_0}(x - x_0 - vt)\right] \tag{5}$$

where

$$\begin{cases} \lambda_0 = \frac{P_s}{L_0}(c\lambda_h + d\lambda_l) \\ \lambda_j = \frac{2}{j\pi}(\lambda_h - \lambda_l)\sin\left(jcP_s\frac{\pi}{L_0}\right) \end{cases} \tag{6}$$

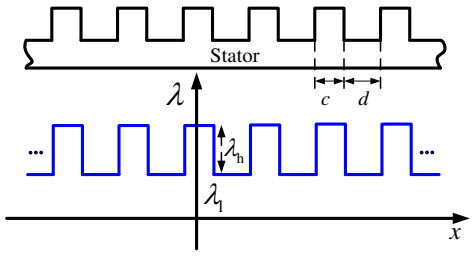

FIGURE 5. Permeance model.

Based on the magnetic circuit method, the air-gap flux density due to PM is equal to the product of the PM MMF drop across the effective machine air gap and effective air-gap permeability.

First, the air-gap flux density of the FSCW machine can be obtained as

$$\begin{aligned} B(x,t) &= F(x)\lambda(x,t) \\ &= F_0\lambda_0 + \lambda_0 \sum_{i=1}^{\infty} F_j \cos\left(iN_s \frac{2\pi}{L_0}x\right) \\ &\quad + \sum_{n=1}^{\infty}\sum_{j=1}^{\infty} F_j\lambda_j \frac{\cos\alpha + \cos\beta}{2} \\ &\quad + F_0 \sum_{j=1}^{\infty} \lambda_j \cos\left[jP_s \frac{2\pi}{L_0}(x - x_0 - vt)\right] \end{aligned} \tag{7}$$

where

$$\begin{cases} \alpha = (iN_s + jP_s)\frac{2\pi}{L_0}x - jP_s\frac{2\pi}{L_0}(x_0 + vt) \\ \beta = (iN_s - jP_s)\frac{2\pi}{L_0}x + jP_s\frac{2\pi}{L_0}(x_0 + vt) \end{cases} \tag{8}$$

According to (8), it can be predicted that the harmonic orders of the flux density include iN_s, jP_s, and $|iN_s \pm jP_s|(i, j = 1, 2, 3\ldots)$.

Similarly, the air-gap flux density due to PMs of the ISDW machine can be expressed as

$$\begin{aligned} B(x,t) &= F(x)\lambda(x,t) \\ &= \lambda_0 \sum_{n=1}^{\infty} F_n \cos\left(nP_m \frac{2\pi}{L_0}x\right) \\ &\quad + \sum_{n=1}^{\infty}\sum_{j=1}^{\infty} F_n\lambda_j \frac{\cos\alpha + \cos\beta}{2} \end{aligned} \tag{9}$$

where

$$\begin{cases} \alpha = (nP_m + jP_s)\frac{2\pi}{L_0}x - jP_s\frac{2\pi}{L_0}(x_0 + vt) \\ \beta = (nP_m - jP_s)\frac{2\pi}{L_0}x + jP_s\frac{2\pi}{L_0}(x_0 + vt) \end{cases} \tag{10}$$

According to (10), it can be predicted that the harmonic orders of the flux density include nP_m and $|nP_m \pm jP_s|(n = 1, 3, 5, j = 1, 2, 3, \ldots)$.

Then, the finite-element method and analytical results of the air-gap magnetic flux density and harmonic order distribution are compared in Figs. 6 and 7. It can be seen that the analytical results show the same trend as the finite element method (FEM) results.

2.3. Performance Comparison

To ensure a fair comparison of the performance between two linear machines, equivalent currents are applied while maintaining consistent usage and effective dimensions of PMs. Fig. 9 shows the single-phase EMF waveforms of the two machines. The back-EMF amplitude of the ISDW machine is approximately 36% higher than that of the FSCW machine. As shown in Fig. 10, the FSCW machine provides 455 N of thrust force, while ISDW machine offers 582 N, representing a thrust force increase of almost 28%. Comparing the slots per phase value the FSCW LPPMV machine is 2/5, and the ISDW LPPMV machine has a unity value of 2, indicating that the ISDW machine has a higher value of Gr. In addition, it can be computed that the Gr of the ISDW machine is more than 1.5 times that of FSCW machine, resulting in a stronger magnetic gear effect and higher back-EMF. These findings suggest that the ISDW machine exhibits a significant advantage over the FSCW machine in terms of thrust performance, given a fixed machine volume, magnetic loading, electrical loading, and the same number of PMs. The average value of self and mutual inductances of the two machines are listed in Table 1. The average self-inductances of the two machines are roughly comparable, meaning that the short-circuit currents are similar, but the ratio of self-inductance to mutual-inductance of ISDW machine is more than three times of the FSCW machine, which indicates that the former has greater interphase coupling and lower fault tolerance. Therefore, it is necessary to solve the problem of low fault tolerance of the ISDW machine.

3. FAULT TOLERANT WINDING CONFIGURATION

Although the ISDW LPPMV machine proposed above has significant advantage in thrust force compared with the FSCW

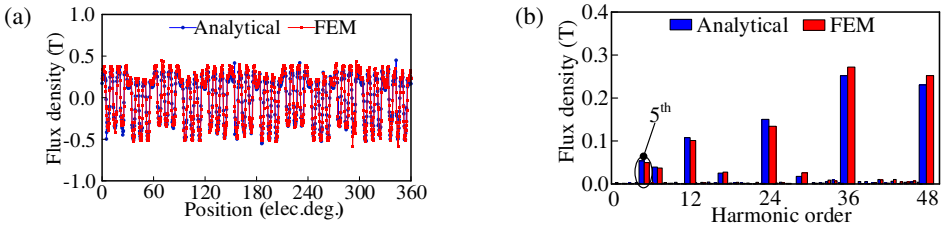

FIGURE 6. Flux density comparison of FSCW machine by analytical and FEM. (a) Waveforms. (b) Harmonic orders.

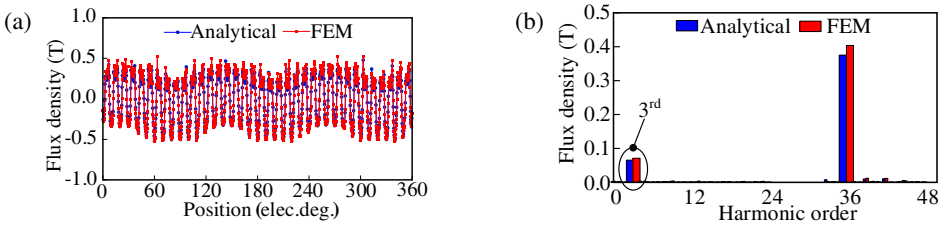

FIGURE 7. Flux density comparison of ISDW machine by analytical and FEMf. (a) Waveforms. (b) Harmonic orders.

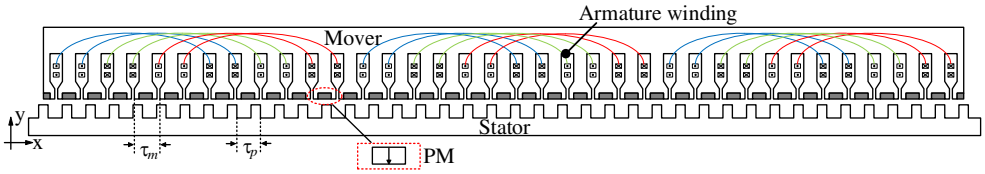

FIGURE 8. Configuration of modular ISDW LPPMV machine.

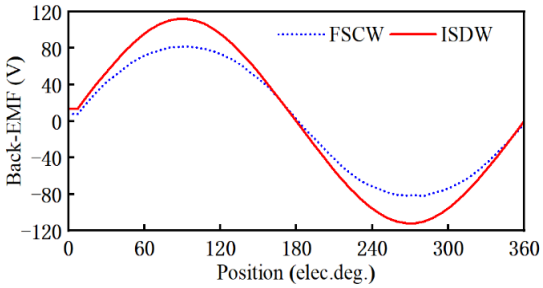

FIGURE 9. No-load back-EMF comparisons of two machines.

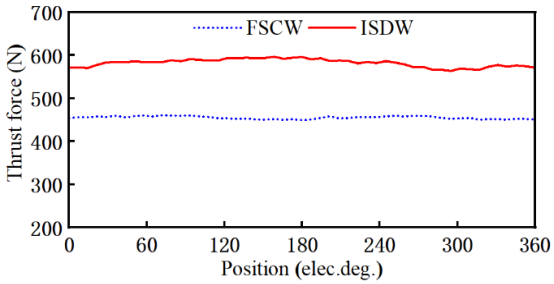

FIGURE 10. Thrust force comparisons of two machines.

LPPMV machine, the fault-tolerant ability needs improvement. For the ISDW machine, in the event of open or short circuit faults occurring in the windings, the three phases are no longer balanced, resulting in great thrust ripple, which makes the machine unable to run. Besides, The windings in different phases of ISDW machine overlap and bundle together, which increases the risk of interphase short circuits. Once the fault has occurred, the heat generated by the faulty phase winding may propagate to other healthy windings through the overlapping windings. Besides, the three-phase windings of the ISDW machine are typically distributed as shown in Fig. 2, in order to achieve a sinusoidal MMF in the air gap, only half of the six slots at each end of the machine are utilized, which reduces the windings utilization.

In order to achieve physical and electrical isolations as well as enhance the winding utilization of the ISDW machine, an isolated triple redundant three-phase winding configuration is proposed. In Fig. 8, the "inter" and "out" directions of the coils in phases B, E, and H are reversed. The ISDW linear machine is divided into three modules with isolated windings. Simultaneously, the induced voltages of phases B, E, and H remain consistent, maintaining balanced three-phase windings in sets ABC, DEF, and GHI. The traditional overlapped winding is divided into three separate three-phase windings, ensuring no contact between them, thereby creating physical and thermal isolation. Electrical isolation is achieved by using three standard inverters to drive each three-phase winding. All six slots at each edge of the machine are utilized. Besides, the MMF distribution and thrust performance of the ISDW machine in healthy

conditions are indeed the same as the original one. Therefore, all advantages of the ISDW are exploited, such as high back EMF and thrust density. Most importantly, the isolated winding brings exceptional fault tolerance, minimizing the risk of fault propagation between different three-phase winding modules and providing redundancy for various faults.

For the modular ISDW linear machine, in order to prevent the occurrence of open-circuit fault in the windings, the faulty three-phase winding can be directly cut off from the power supply. The remaining two healthy three-phase sets can continue to operate, albeit with a reduced thrust force or power output of approximately one-third. In the case of a short-circuit fault in one of the three-phase windings, the faulted group can be subjected to terminal short-circuiting by closing the corresponding top or bottom switches of the three-phase inverters. Due to the significant self-inductance inherent in field-modulated linear machines, the short-circuit current will be lower than the rated value. Consequently, due to the separation of windings, a fault within one three-phase system can be isolated, allowing the other two sets to continue operating and transmitting thrust or power.

4. PERFORMANCE EVALUATION

In this section, the performance of the modular ISDW linear machine under normal condition is evaluated in order to enable comparisons with its performance under fault conditions in subsequent sections. Unless stated otherwise, all the assessments are conducted at a base speed of 1.5 m/s. In general, it is assumed that the faults include open circuit and short circuit, both occurring in the ABC three-phase windings. It is remarkable that the modular ISDW machine in this article has been optimized. Due to the limited space of the article and the focus of this article not on the optimization of the machine, the specific optimization process will not be described in detail.

4.1. Back EMF and Thrust Force

The back EMFs of modular ISDW LPPMV machine are shown in Fig. 11. Since the back EMFs of all three sets are identical, only ABC winding is displayed. Due to minimal harmonic content in the air gap when the machine is operating under no-load conditions, the three-phase back-EMF waveforms are sinusoidal. Furthermore, the amplitude of the three-phase back EMFs of modular ISDW machine is 46 V, which is significantly higher than one-third of the ISDW LPPMV machine.

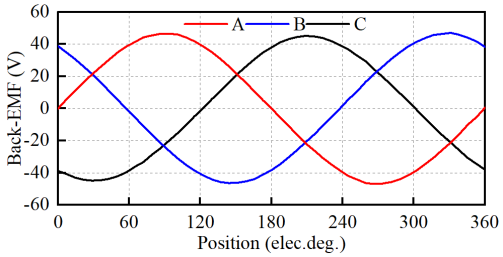

FIGURE 11. Back EMF of modular ISDW machine at 1.5 m/s.

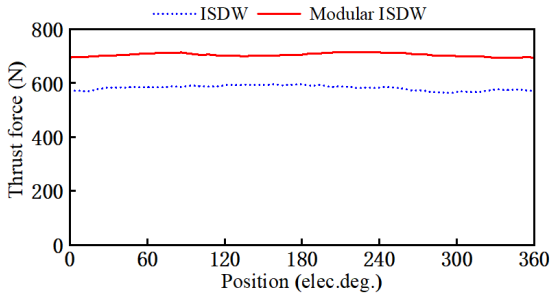

FIGURE 12. Thrust force in healthy condition.

The thrust force waveform of ISDW LPPMV machine and modular one is shown in Fig. 12. The former is composed of one set three-phase winding, and the latter consists of three sets three-phase windings. Both machines are operating at a rated current of 5 A under normal conditions. The modular ISDW LPPMV machine has outputted an average thrust of 705 N, which is 21% higher than that before the winding configuration. Fig. 13 shows detent force of the modular ISDW machine, and the amplitude is insignificant compared to the thrust force. As the end-winding and slotting forces of ISDW LPPMV machine are smaller than those in traditional linear machines, its overall thrust ripple performance is relatively better.

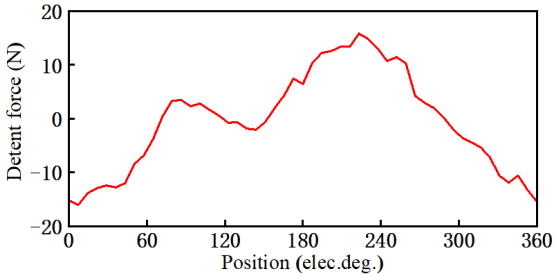

FIGURE 13. Detent force of modular ISDW machine.

Figure 14 shows the 2D flux distribution of modular ISDW machine under rated conditions, which conspicuously repeats periodically three times along the effective length. It can be predicted that the magnetic flux distribution of the three sets is also identical under healthy conditions.

4.2. One Set Open Circuit

Figure 15 shows the thrust of the ISDW LPPMV machine and the modular one in heathy condition, set ABC open circuited and fault-tolerant operation. It is obvious that the ISDW machine cannot work under open circuited condition due to the huge thrust ripple result from unbalanced three phase winding. Besides, one set of three-phase windings means that the ISDW machine does not have the ability to operate fault-tolerant. For the modular ISDW machine, when a winding discontinuity, switch disconnection, or control fault occurs, all inverter switches should be opened to render the faulted phase group ineffective. The current of the faulty set reaches zero. The remaining two sets of three-phase windings are excited with the same current to generate the thrust force. The thrust force of

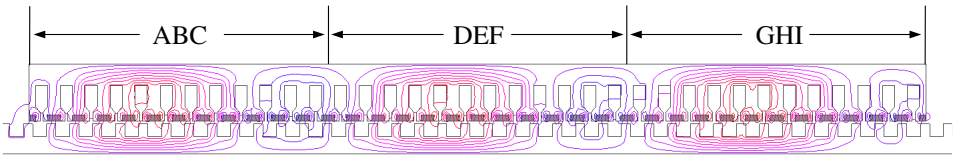

FIGURE 14. Flux distribution in healthy condition.

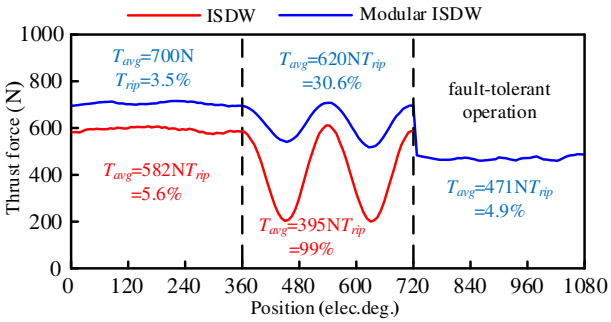

FIGURE 15. Thrust force with set ABC open circuited.

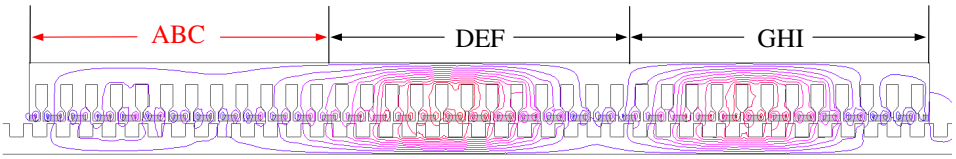

FIGURE 16. Flux distribution with set ABC open circuited.

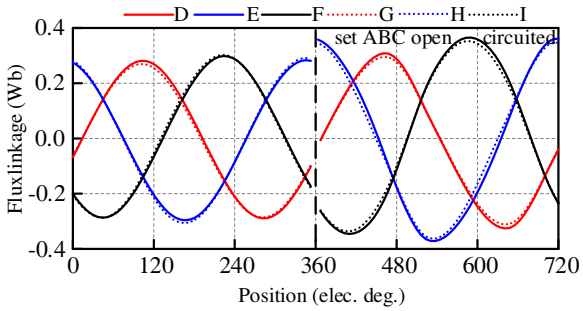

FIGURE 17. Phase flux linkages of DEF and GHI in healthy condition and set ABC open circuited.

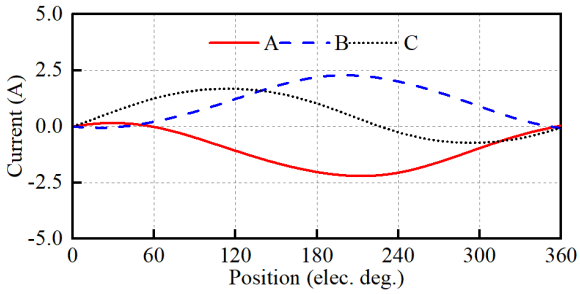

FIGURE 18. Short-circuit phase currents.

the modular ISDW machine is 471 N in fault-tolerant operation, basically equal to 2/3 of the rated value.

The magnetic flux distribution under open-circuit conditions for the ABC winding can be observed in Fig. 16. In addition to a reduction in the magnitude of the 3rd harmonic wave due to fault conditions, there are also partial increases in the magnitudes of the 1st and 2nd harmonics, which collectively contribute to thrust ripple during fault-tolerant operation. Besides, it also shown that the flux linage in the remaining two heathy modules region is basically unaffected. Therefore, the other two sets of windings will not be affected to continue the load reduction operation.

Figure 17 shows the flux linkage waveforms of phases DEF and GHI under healthy and ABC set open circuited conditions. The flux linkages of the two 3-phase sets are basically identical to set ABC in the initial machine cycle. In the second machine cycle, the flux linkage waveforms of phases DEF and GHI are slightly unbalanced. The distortion in the flux linkage waveforms varies among different phases due to the imbalance. The distortion in the D phase waveform is minimal, while there is slightly more distortion in the E and F phases, primarily at-

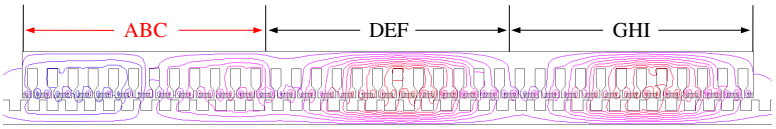

FIGURE 19. Flux distribution with set ABC short circuited.

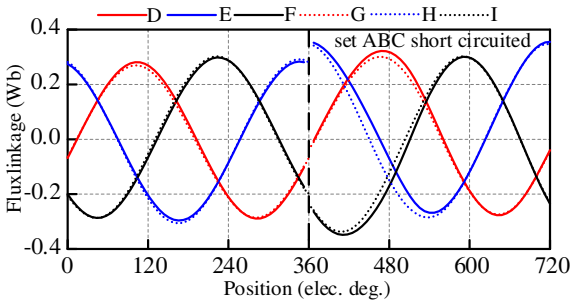

FIGURE 20. Phase flux linkages of DEF and GHI in healthy condition and set ABC short circuited.

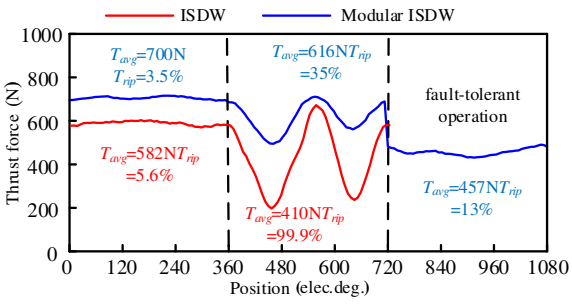

FIGURE 21. Thrust force with set ABC short circuited.

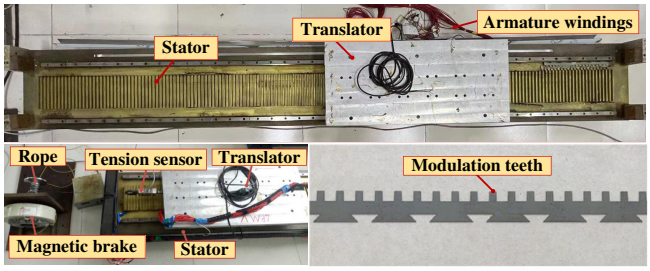

FIGURE 22. Experimental platform. Prototype of the modular ISDW LPPMV machine.

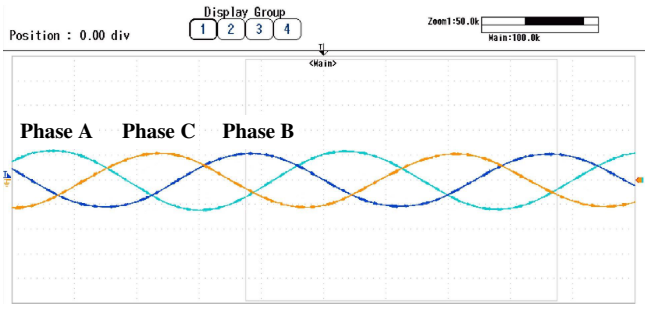

FIGURE 23. No-load back EMF of measured.

tributed to linear spatial position, the physical proximity of the E and F phases to the open-circuit ABC phases.

4.3. One Set Short Circuit

In the event of a switch within the inverter, or one phase winding is short-circuited, that specific inverter should open all its top or bottom switches to apply terminal short-circuit to the faulty winding. Similar to the case of single-phase open circuit, the healthy two three-phase sets continue to operate. Fig. 18 shows the resulting short circuited phase currents, which are lower than the rated value due to the relatively low PM flux and higher self-inductance of the LPPMV machine. Therefore, the faulty three-phase set will not generate excessive heat, and the machine will continue to operate safely. It can be observed that the short-circuit currents of the ABC windings are asymmetrical, which is caused by the incomplete isolation between the healthy and faulty windings, resulting in mutual coupling.

Figure 19 shows the flux distribution under short-circuit condition. It can be observed that the magnetic flux within the region occupied by the short-circuited ABC group is almost entirely canceled out by the short-circuit currents. The magnetic flux density within this region is very low. Conversely, the magnetic flux density distributions in regions DEF and GHI are almost normal, as clearly seen from the magnetic flux waveform depicted in the second machine cycle in Fig. 20.

The thrust force of the ISDW LPPMV and the modular ISDW LPPMV in heathy condition, set ABC short circuited and fault-tolerant operation are depicted in Fig. 21. Similarly, the thrust force of the modular ISDW machine under fault-tolerant condition is 457 N, slightly lower than two-thirds of the rated thrust force and the thrust force waveform under open-circuit conditions. The thrust force ripple is also slightly higher than that under open-circuit conditions. These results confirm that the proposed machine can accommodate short-circuit faults.

5. EXPERIMENTAL VERIFICATION

In order to verify the conclusion of finite element analysis, an ISDW LPPMV machine with 3 × 3-phase modular windings depicted in Fig. 22 has been designed and manufactured. The stator and mover of the machine are composed of stacked silicon steel sheets, and the secondary comprises 39 effective modulation teeth. To facilitate machining and installation, the bot-

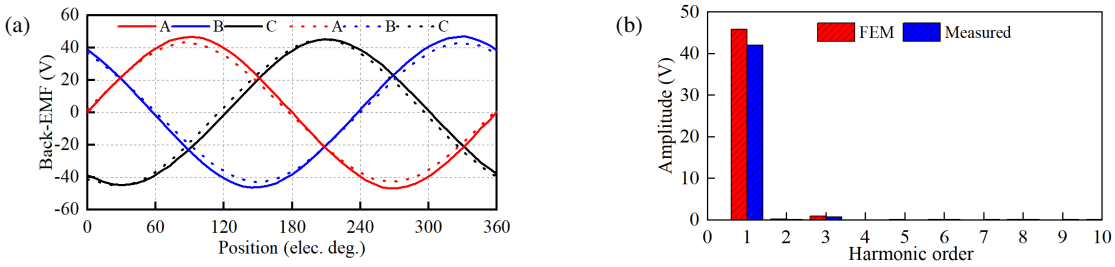

FIGURE 24. Comparison of FEM and measured back EMFs. (a) Waveform. (b) Harmonic order.

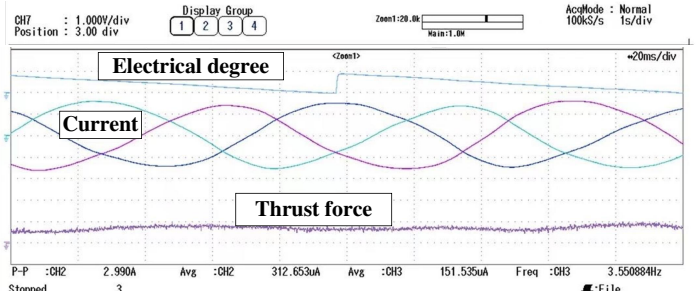

FIGURE 25. Measured thrust force and currents.

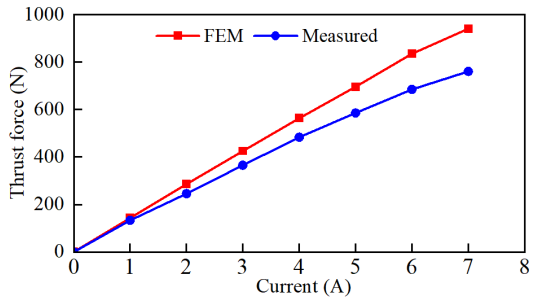

FIGURE 26. Predicted and experiment thrust force variations with current.

tom end of the stator teeth is designed into a dovetail structure. A nine-phase inverter configured as three independent three-phase sets has also been developed to drive the machine, utilizing a digital signal processing (DSP) control board.

In the no-load experiment of linear machine, a rotary motor is first needed to provide traction. The rotary motor is coaxial with the rotating axis of the magnetic brake. The linear machine is connected to the magnetic brake by a rope. By adjusting the rotation speed of the rotary motor, the machine moves at a speed of 1.5 m/s in the horizontal direction. Fig. 23 shows the waveform of the experimental back EMF measured at 1.5 m/s. For simplicity, only the experimental back EMF of module ABC is depicted. As shown in Fig. 24(a), the measured back-EMF waveform of phase ABC was symmetric and sinusoidal, basically consistent with the finite element analysis results. The no-load back-EMF harmonic analysis of phase A is shown in Fig. 24(b). The fundamental values of the finite element and experimental measurements are 46 and 42 V volts, respectively. In addition, the amplitude of other harmonics is also very similar.

Figure 25 shows the measured thrust force and current waveform of the machine. The measured average thrust force is recorded at 680.6 N, which is lower than that of average thrust force given by FEM. This may be due to experimental errors, but the loss of thrust force is acceptable. The experimental and simulated results of the proposed ISDW LPPMV machine are presented in Table 2. Fig. 26 compares the experimented and predicted thrust forces of the LPPMV machine variations with current. It can be seen that when the input current value is low, the difference between the experimental value and predicted value is small, but with the increase of the input current, the deviation also increases. It may be that the magnetic circuit is saturated due to the temperature rise generated by the machine during the experiment.

TABLE 2. Comparison of FEM and measured values.

Parameters	FEM	Measured	Percentage deviation(%)
Phase A(V)	46.5	42.7	8.2
Phase B(V)	45.6	41.1	9.9
Phase C(V)	45.2	41.8	7.5
Thrust force(N)	705	680.6	3.5

The prototype drive system has been tested under open and short circuits in one three-phase set ABC. During the test, open and short circuits occurred only in set ABC, and the remaining three-phase sets DEF and GHI were independently controlled with the same rated current under healthy conditions. Fig. 27 shows the comparison of thrust forces under opened and shorted circuits with healthy conditions as changes of the current. It can be seen that the machine can provide 69% of the thrust in health when it is open circuit. Besides, the thrust force under ABC set

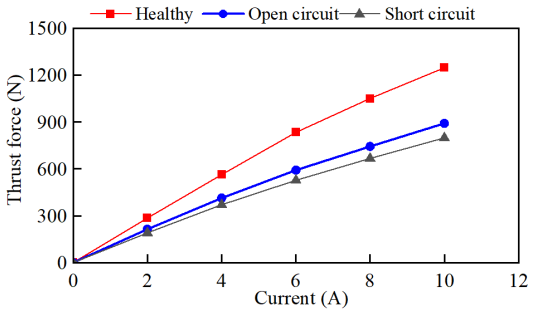

FIGURE 27. Thrust force comparison with set ABC open and short circuited.

short circuited is close to 65% of the thrust force in the healthy condition, and it is basically equal to the predicted value.

6. CONCLUSION

In this paper, an ISDW LPPMV machine with high modulation ratio was proposed. First, the performances of ISDW machine and conventional FSCW machine were compared. The ISDW machine exhibits significantly higher thrust force characteristics. Then, the thrust force density improvement mechanism was revealed from the perspective of contribution of flux density harmonics. Furthermore, in order to improve the fault tolerance and winding utilization of ISDW machine, a modular ISDW LPPMV machine is newly proposed and optimized. Due to the improvement of wingding utilization, the thrust force of the modular LSDW LPPMV machine is significantly increased. Besides, the fault performance was analyzed and compared in open-circuit and short-circuit conditions. Finally, the predicted performances of the proposed modular ISDW machine were validated by experiments on a prototype machine.

ACKNOWLEDGEMENT

This work was supported in part by the National Natural Science Foundation of China under Projects 52307057 and 52207056, in part by the Natural Science Foundation of Jiangsu Province under Grant BK20230539, and in part by the Key Research and Development of Zhenjiang under Grant GY2023011.

REFERENCES

[1] Shen, Y., Z. Li, Z. Zeng, Q. Lu, and C. H. T. Lee, "Quantitative analysis of asymmetric flux reversal permanent magnet linear machine for long excursion application," *IEEE Transactions on Industrial Electronics*, Vol. 71, No. 10, 12 781–12 792, 2024.

[2] Zhao, X., C. Wen, M. Li, Q. Zhao, K. Lv, and X. Wang, "Research on efficiency optimization based on permanent magnet synchronous linear motor," *Progress In Electromagnetics Research Letters*, Vol. 101, 147–155, 2021.

[3] Zhi, R., B. Liu, G. Lv, L. Cui, and T. Zhou, "Characteristics analysis of novel transverse flux linear synchronous motor for maglev transportation," *IEEE Transactions on Transportation Electrification*, Vol. 9, No. 3, 4104–4112, 2023.

[4] Wen, C., J. Chen, J. Cui, Z. Wan, and Y. Chang, "Optimization of electromagnetic thrust for short primary unilateral linear induction motor," *Progress In Electromagnetics Research C*, Vol. 142, 75–83, 2024.

[5] Shiri, A. and A. Tessarolo, "Normal force elimination in single-sided linear induction motor using design parameters," *IEEE Transactions on Transportation Electrification*, Vol. 9, No. 1, 394–403, 2023.

[6] Shen, Y., Q. Lu, and Y. Li, "Design criterion and analysis of hybrid-excited Vernier reluctance linear machine with slot Halbach PM arrays," *IEEE Transactions on Industrial Electronics*, Vol. 70, No. 5, 5074–5084, 2023.

[7] Liu, G., H. Zhong, L. Xu, and W. Zhao, "Analysis and evaluation of a linear primary permanent magnet vernier machine with multiharmonics," *IEEE Transactions on Industrial Electronics*, Vol. 68, No. 3, 1982–1993, 2021.

[8] Zhou, Y., R. Qu, D. Li, Y. Gao, and C. H. T. Lee, "Performance investigation and improvement of linear vernier permanent magnet motor for servo application," *IEEE/ASME Transactions on Mechatronics*, Vol. 28, No. 5, 2657–2669, 2023.

[9] Zhao, W., T. Yao, L. Xu, X. Chen, and X. Song, "Multi-objective optimization design of a modular linear permanent-magnet vernier machine by combined approximation models and differential evolution," *IEEE Transactions on Industrial Electronics*, Vol. 68, No. 6, 4634–4645, 2021.

[10] Ge, Q., B. Kou, H. Zhang, Y. Shao, C. Huang, and X. Niu, "Secondary eddy current losses reduction in a double-sided long-primary fractional slot concentrated winding permanent magnet linear synchronous motor," *IEEE Transactions on Industrial Electronics*, Vol. 69, No. 5, 5018–5029, 2022.

[11] Ge, J., W. Xu, Y. Liu, F. Xiong, and D. Li, "Investigation on winding theory for short primary linear machines," *IEEE Transactions on Vehicular Technology*, Vol. 70, No. 8, 7400–7412, 2021.

[12] Sun, Z., Q. Wang, Z. Qian, and G. Li, "Estimate end-winding temperature for water-cooled interior permanent magnet motors under variable-speed driving cycles: A solution to the exact challenge," *IEEE Transactions on Transportation Electrification*, Vol. 9, No. 1, 370–381, 2023.

[13] Zhang, Z., C. Wang, and W. Geng, "Design and optimization of halbach-array pm rotor for high-speed axial-flux permanent magnet machine with ironless stator," *IEEE Transactions on Industrial Electronics*, Vol. 67, No. 9, 7269–7279, 2020.

[14] Mao, Y., Z. Sun, C. Huang, G. Jia, and A. Ding, "Electromagnetic characteristics analysis of a novel ironless double-sided halbach permanent magnet synchronous linear motor for electromagnetic launch considering longitudinal end effect," *IEEE Transactions on Transportation Electrification*, Vol. 10, No. 3, 7467–7477, 2024.

[15] Zhao, W., J. Zheng, J. Wang, G. Liu, J. Zhao, and Z. Fang, "Design and analysis of a linear permanent-magnet vernier machine with improved force density," *IEEE Transactions on Industrial Electronics*, Vol. 63, No. 4, 2072–2082, 2016.

[16] Huang, X., T. Ji, L. Li, B. Zhou, Z. Zhang, D. Gerada, and C. Gerada, "Detent force, thrust, and normal force of the short-primary double-sided permanent magnet linear synchronous motor with slot-shift structure," *IEEE Transactions on Energy Conversion*, Vol. 34, No. 3, 1411–1421, 2019.

[17] Wen, C., J. Cui, M. Li, Z. Wan, and Y. Chang, "Co-optimization of long secondary double-sided linear flux switching permanent magnet motors," *Progress In Electromagnetics Research C*, Vol. 141, 101–108, 2024.

[18] Ma, A., W. Zhao, L. Xu, J. Ji, and F. Bian, "Influence of armature windings pole numbers on performances of linear permanent-magnet vernier machines," *IEEE Transactions on Transporta-*

tion Electrification, Vol. 5, No. 2, 385–394, 2019.

[19] Wu, L., R. Qu, D. Li, and Y. Gao, "Influence of pole ratio and winding pole numbers on performance and optimal design parameters of surface permanent-magnet vernier machines," *IEEE Transactions on Industry Applications*, Vol. 51, No. 5, 3707–3715, 2015.

[20] Xu, L., G. Liu, W. Zhao, J. Ji, H. Zhou, W. Zhao, and T. Jiang, "Quantitative comparison of integral and fractional slot permanent magnet vernier motors," *IEEE Transactions on Energy Conversion*, Vol. 30, No. 4, 1483–1495, 2015.

[21] Liu, Y. and Z.-Q. Zhu, "Influence of gear ratio on the performance of fractional slot concentrated winding permanent magnet machines," *IEEE Transactions on Industrial Electronics*, Vol. 66, No. 10, 7593–7602, 2019.

[22] Wang, S., W. Zhao, J. Ji, L. Xu, and J. Zheng, "Magnetic gear ratio effects on performances of linear primary permanent magnet vernier motor," *IEEE Transactions on Applied Superconductivity*, Vol. 26, No. 7, 1–5, 2016.

[23] Xu, B., Q. Wu, J. Ma, L. Wu, L. Qiu, X. Liu, and Y. Fang, "Research on the influence of end turn length on consequent-pole vernier permanent-magnet machines," *IEEE Transactions on Magnetics*, Vol. 58, No. 8, 1–9, 2022.

[24] Wang, B., C. Zha, Y. Xu, J. Wang, M. Cheng, and W. Hua, "Comparative study on fault-tolerant triple three-phase PM machine drive with five modular windings," *IEEE Transactions on Industrial Electronics*, Vol. 70, No. 10, 9720–9730, 2023.

[25] Wang, R., D. Li, X. Fan, R. Qu, S. Yang, P. Wang, and R. Li, "Analysis of short-circuit current automatic suppression for toroidal winding PM machines," *IEEE Transactions on Power Electronics*, Vol. 39, No. 6, 7510–7524, 2024.

[26] Zhao, M., G. Liu, X. Wang, J. Mao, J. Zheng, and X. Zhu, "Fault-tolerant sensorless control for a 3×3-phase pma-synrm based on frequency adaptive extended-state-observer," *IEEE Transactions on Transportation Electrification*, 1–1, 2024.